Detection Rates for Close Binaries Via Microlensing

B. Scott Gaudi

Andrew Gould[1]

Dept of Astronomy, Ohio State University, Columbus, OH 43210

e-mail gaudi@payne.mps.ohio-state.edu

e-mail gould@payne.mps.ohio-state.edu

Abstract

Microlensing is one of the most promising methods of reconstructing the stellar mass function down to masses even below the hydrogen-burning limit. The fundamental limit to this technique is the presence of unresolved binaries, which can in principle significantly alter the inferred mass function. Here we quantify the fraction of binaries that can be detected using microlensing, considering specifically the mass ratio and separation of the binary. We find that almost all binary systems with separations greater than $b \sim 0.4$ of their combined Einstein ring radius are detectable assuming a detection threshold of 3%. For two M dwarfs, this corresponds to a limiting separation of $\gtrsim$ 1AU. Since very few observed M dwarfs have companions at separations $\lesssim$ 1AU, we conclude that close binaries will probably not corrupt the measurements of the mass function. We find that the detectability depends only weakly on the mass ratio. For those events for which individual masses can be determined, we find that binaries can be detected down to $b \sim 0.2$.

---

1 Alfred P. Sloan Foundation Fellow

1. Introduction

Four surveys are currently discovering microlensing events towards the Large Magellenic Cloud and the galactic bulge (Alcock et al. 1996; Aubourg et al. 1995; Udalski et al. 1994; Alard 1996). While the initial goal of these surveys was to determine the fraction of the halo that is composed of massive compact halo objects, the possible returns on these surveys are much broader. In particular, it may soon be possible to measure the mass function of the lenses.

Traditional methods of measuring the stellar mass function are restricted to luminous objects. Thus these methods can only be applied to stars above the hydrogen-burning limit, and are restricted to sparse samples near this limit. Microlensing overcomes this limitation because the effect is due to the mass of the lens, not its intrinsic luminosity. Thus microlensing samples can extend mass function measurements beyond the hydrogen-burning limit.

In general it is not possible to measure the masses of individual microlenses. This is because the only parameter that yields any information about the lens is the timescale t_e, given by,

$$t_e = \frac{r_e}{v}, \tag{1.1}$$

where v is the transverse velocity of the lens relative to the observer-source line of sight, and r_e is the Einstein ring radius,

$$r_e^2 = \frac{4GM}{c^2} D_{\mathrm{OS}}\, z(1-z), \;\; z = \frac{D_{\mathrm{OL}}}{D_{\mathrm{OS}}}. \tag{1.2}$$

Here D_{OL}, D_{OS}, and D_{LS} are the distance between the observer, lens, and source, and M is the mass of the lens. Thus t_e is a complicated function of the quantities of interest: the mass, velocity, and distance of the lens. There are two basic methods of acquiring additional information. The first is using parallax to measure the projected Einstein radius of the lens, $\tilde{r}_e = (D_{\mathrm{OS}}/D_{\mathrm{LS}})r_e$, either by considering the parallax caused by the motion of the Earth (Gould 1992; Alcock et al. 1995;

Buchalter & Kamionkowski 1996), or by employing a parallax satellite (Refsdal 1966; Gould 1995a; Boutreux & Gould 1996; Gaudi & Gould 1996). The second method is using proper motion information to measure the angular Einstein radius, $\theta_e = 4GM/c^2 \tilde{r}_e$ (Gould 1994; Nemiroff & Wickramasinghe 1994; Witt & Mao 1994; Gould & Welch 1996). Combining these two pieces of information yields the mass, distance and velocity of the lens (Gould 1996a and references therein). Gould (1995b) estimates that one can expect ~ 100 giant events towards the galactic bulge per year. A parallax satellite would be able to measure parallaxes for $\sim 70\%$ of these events (Gaudi & Gould 1996), and $\sim 15\%$ of events could yield proper motions with current technology (Gould 1996a). Thus one might expect to obtain full information for ~ 15 events per year.

The fundamental limitation to using microlensing to reconstruct the mass function comes from the issue of unresolved binaries. If one assumes that the individual masses measured are due to single lenses without considering unresolved binaries, the reconstructed mass function will be biased toward large masses. This issue has been studied for the stellar mass function as determined from counts of luminous stars in the solar neighborhood (Reid 1991; Kroupa et al. 1991), and it has been shown that unresolved binaries can significantly alter the inferred mass function, in particular leading to an underestimation of the numbers of low-mass stars. Unresolved binaries could pose a similar problem for microlensing. It is thus important to quantify the detectability of binaries from microlensing.

Binary events can be divided into three basic classes according to the separation, b, in units of the Einstein ring radius: wide binaries ($b \gg 1$), intermediate binaries ($b \sim 1$), and close binaries ($b \ll 1$). Although it may be difficult to determine the frequency of wide binaries from microlensing experiments, these objects pose no problem for reconstructing the mass function because the light curve for each member is unaffected by the presence of the other. Similarly, intermediate binaries pose no difficulty because they give rise to events that deviate dramatically from those of single lenses, and hence are easily distinguished. However, close binaries are problematic in that they can masquerade as point lenses. In this way

microlensing differs from traditional methods of detecting binaries: the closer a companion is to a luminous star, the larger the induced orbital motion and hence the *easier* it is to detect spectroscopically.

The goal of this paper is to quantify the fraction of binary microlensing events for which the binarity of the lens is detectable. We specifically focus on close binaries, for which $b \leq 1$. In particular we quantify the smallest separation that can be resolved for a majority of events given specified observing parameters. We also discuss the effects of the mass ratio of the binary components and effects of finite source size on the detectability.

2. Observed Frequencies of Close Binaries

Before calculating detection rates, we first review what is known about the frequency of close binaries, specifically for low-mass stars and brown dwarfs, where microlensing is most useful. Unfortunately, there is no information about the binarity of objects with masses below the hydrogen-burning limit, the regime of greatest interest. The most relevant observed sample is of the stars just above the hydrogen-burning limit. Various surveys of local, late-type dwarf stars have been made with the aim of discovering unseen companions. Precise radial velocity measurements are the most sensitive to low-mass, close binaries. Marcy & Benitz (1989) obtained radial velocity measurements of M dwarfs in the solar neighborhood, with precisions of $\sim 200\,\mathrm{m\,s^{-1}}$, allowing detection of companions with masses $\gtrsim 0.01 M_\odot$. Fischer & Marcy (1992) examined this sample, and found that out of 62 primaries, only three have a companions with separations of $\lesssim 1\mathrm{AU}$. They estimate a detection probability of 86% for this range. For two M dwarfs, 1AU corresponds to a separation in units of the Einstein ring radius of $b \sim 0.4$. Thus approximately $3/(.86 \times 62) \sim 6\%$ of M dwarfs in the solar neighborhood have companions with $b < 0.4$. Although the solar neighborhood may not be a perfectly representative sample, it appears that binaries with separations $b < 0.4$ are not common. As we show below, with observations of reasonable photometric precision, almost all

4

binaries with separations $b > 0.4$ are detectable. Moreover, we show that for events where the mass can actually be measured, binarity is detectable even at substantially smaller separations. Thus close binaries are unlikely to be a major source of error for reconstructing the mass function via microlensing.

3. Binary Lensing Formalism

Consider a binary lens system. The Einstein ring radius for the binary system is given by equation (1.2), where M now denotes the total mass of the binary. We will normalize all subsequent lengths and masses to r_e and M. Using complex coordinates, we denote the position of the source with respect to the center of mass of the binary as $\zeta = \xi + i\eta$, and the position of the component masses m_1 and m_2 as z_1 and z_2. The image positions, $z = x + iy$, are then given by (Witt 1990),

$$\zeta = z + \frac{m_1}{\bar{z}_1 - \bar{z}} + \frac{m_2}{\bar{z}_2 - \bar{z}}. \tag{3.1}$$

The magnification, A_i, of each image is given by the Jacobian of the transformation (3.1), evaluated at the image position,

$$A_i = \frac{1}{|\det J|}\Bigg|_{z=z_i}, \quad \det J = 1 - \frac{\partial \zeta}{\partial \bar{z}}\overline{\frac{\partial \zeta}{\partial \bar{z}}}. \tag{3.2}$$

If the images are unresolved, the total magnification is given by the sum of the individual magnifications, $A = \sum A_i$. The set of source positions where the magnification is formally infinite, given by the condition $\det J = 0$, define closed curves called caustics. Five images are created if the source is inside a caustic, three if the source is outside. It is those regions near the caustics where the magnification from the binary deviates most dramatically from that of a point lens.

In practice, equation (3.1) is solved numerically in order to determine the image positions, and these positions, together with equation (3.2), are then used to calculate the total magnification.

4. Detection Rates

After normalizing to r_e and M, there are two parameters that determine the lensing structure of a binary: b, the binary separation, and the mass ratio, $q = m_1/m_2$. To analyze how the magnification of a binary lens deviates from that of a point mass lens for a specified q and b, we define ϵ, the excess magnification over a single lens,

$$\epsilon = \frac{A - A_0}{A_0}, \tag{4.1}$$

where A_0 is the magnification of a point lens with mass equal to the total mass of the binary, M, and located at the center of mass of the binary,

$$A_0 = \frac{|\zeta|^2 + 2}{|\zeta|\,(|\zeta|^2 + 4)^{1/2}}. \tag{4.2}$$

We then calculate ϵ as a function of the source position, (ξ, η), and draw contours of $\epsilon = \pm 3\%, \pm 10\%$. These excess magnification contours define regions where the magnification of the binary lens deviates from that of the single lens by 3% and 10%. Figure 1 shows contours of ϵ for $q = 0.1, 0.4, 0.7, 1.0$ and $b = 0.2, 0.3, 0.4, 1.0$.

Ignoring higher-order effects (unresolved light from unmagnified sources, finite source, etc.), there are six parameters that characterize a binary lens event. Two of these are intrinsic to the lens: b and q. Three are purely geometrical factors that describe the lens trajectory: t_0, the time of closest approach of the source and the center of mass of the lens, β, the separation between the source and center of mass at t_0, and θ, the angle that the lens trajectory makes with the projected binary axis. The final parameter is the timescale of the event, given by equation (1.1). A lensing event will be a straight line through the maps of ϵ, specified by these six parameters. We want to know, given any event being observed with a specified sampling rate, n_{meas}, what is the probability of distinguishing a binary with parameters q and b from a point-mass lens. This means we must consider all
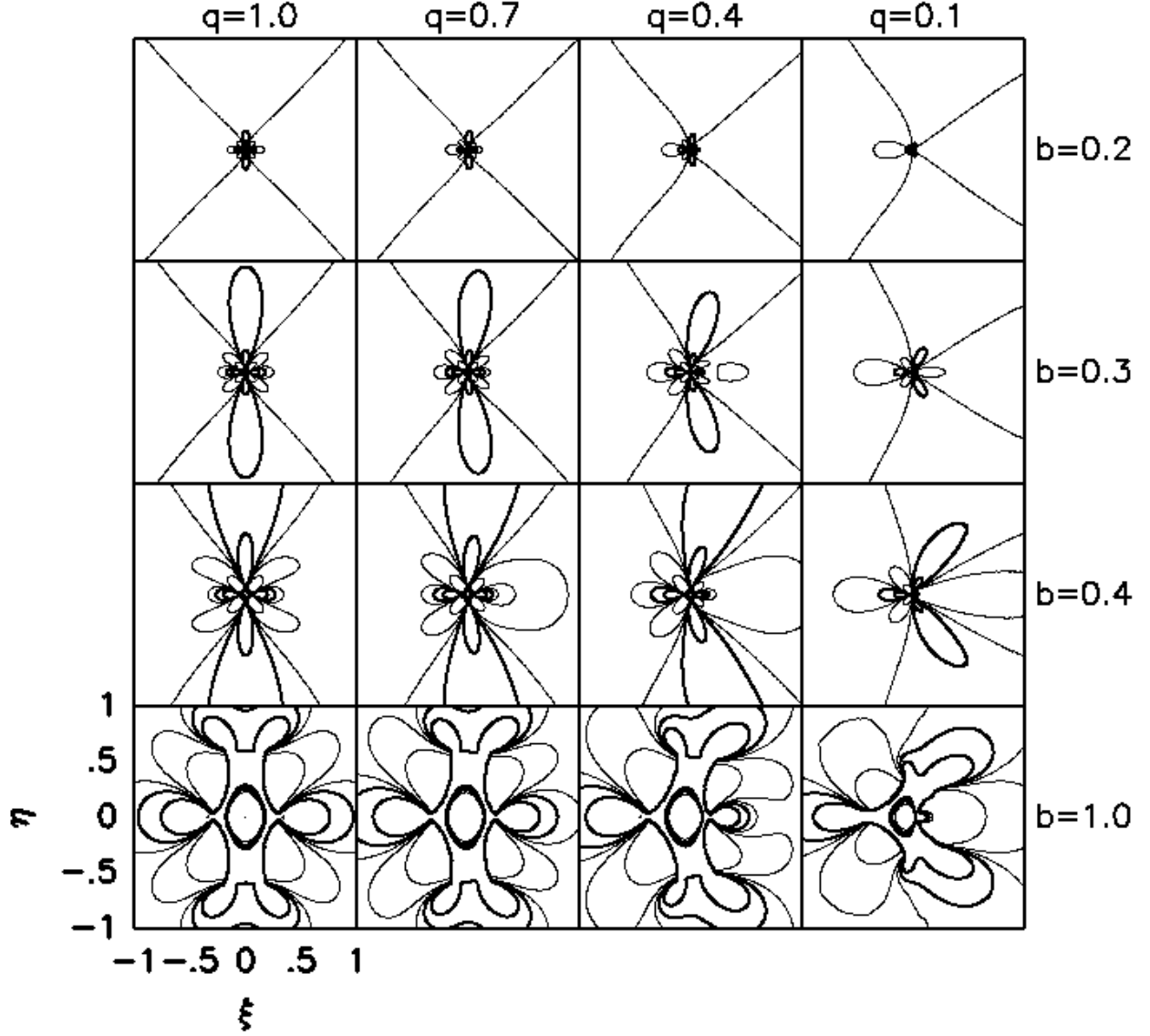
Figure 1. Contours of excess magnification, $\epsilon = 0, \pm 0.03, \pm 0.10$, for four values of b, the binary separation in units of the Einstein ring, and q, the ratio of the masses of the binary components. Positive contours are bold.

possible β and θ. Since t_0 has no effect on the detection probability, we ignore it. For each possible trajectory, we ask whether, at each measurement, $|\epsilon| \geq \epsilon_{thres}$, where ϵ_{thres} is the given detection threshold. If this requirement is met, we consider

that the binary has been detected. The distributions of β and θ are flat. We therefore integrate over all trajectories with $0 \le \beta \le 1$ and $0 \le \theta \le 2\pi$. The probability for detecting the binary is simply the ratio of the number of events for which the binary was detected to the total number of trial events. Comparing the panels of Figure 1, it is apparent that the binary detection probability depends much more strongly on b than q. For $b = 1.0$, nearly all possible event trajectories will cross contours of 3%, and therefore the fraction of events for which the binary is detected is ~ 1, whereas for $b = 0.2$, the fraction of events for which the binary is detected is $\ll 1$. For $b = 0.4$, a significant fraction of trajectories will still cross contours of 3%. This implies that the binary detection probability must decline rapidly from $b = 0.4$ to $b = 0.2$.

In order to calculate binary detection probabilities, we adopt parameter values $\epsilon_{thres} = 3\%$ and 10%, and $n_{meas} = 25$ measurements per r_e. For $D_{OS} \sim 8 \, \text{kpc}$ and $D_{OL} \sim 4 \, \text{kpc}$,

$$r_e \sim 4 \, \text{AU} \left(\frac{M}{M_\odot} \right)^{1/2}. \tag{4.3}$$

Thus for a binary consisting of two M stars, $M \sim 0.4 M_\odot$, $r_e \sim 3 \, \text{AU}$. Assuming $v \sim 200 \, \text{km s}^{-1}$, then $t_e \sim 25 \, \text{days}$. Therefore n_{meas} corresponds to one measurement per day. In fact, our results are rather insensitive to choice of n_{meas}, since, from Figure 1, for $b \ge 0.3$, the regions of $\epsilon > 0.1$ are all larger than $\sim 0.1 r_e$, and therefore the binary will be detected for any $n_{meas} > 10$. Furthermore, current follow-up surveys have temporal resolutions much greater than those used in our calculations.

Figure 2 shows contours of binary detection probability as a function of b and q for $\epsilon_{thres} = 10\%$. As expected, P is much more sensitive to b than q, and declines rapidly for $b \lesssim 0.5$. Excess magnification contours of $\epsilon = 0.10$ follow closely the structure of the caustics. Thus we can examine the structure of the caustics to understand Figure 2. In Figure 3, we show the caustics for three binary separations. For separations of $0.7 \lesssim b \le 1.0$, there is only one caustic, and the binary detection
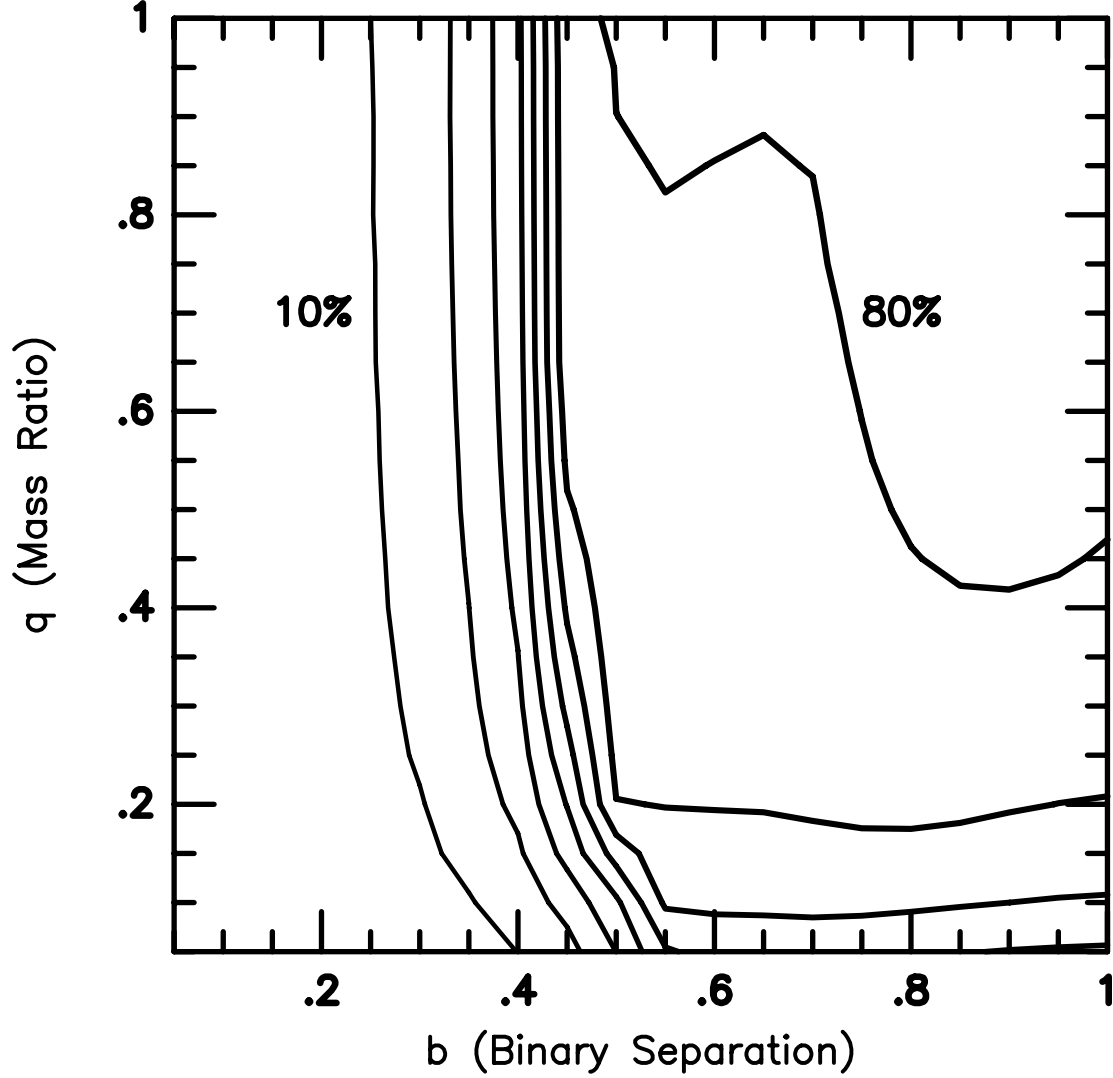
Figure 2. Contours of detection probability as a function of binary separation and mass ratio for $\epsilon_{thres} = 0.10$. Contours have equal spacings of 10%. A binary is considered detected if $|\epsilon| > 0.10$ at any point during the event.

probability is roughly given by the cross section of this caustic integrated over all angles θ. At a binary separation of $b = 2^{-1/2} \simeq 0.7$, the caustics splits into three parts. The main, diamond-shaped caustic is located near the center of mass, and the two smaller triangle-shaped caustics are on the η axis symmetrically above
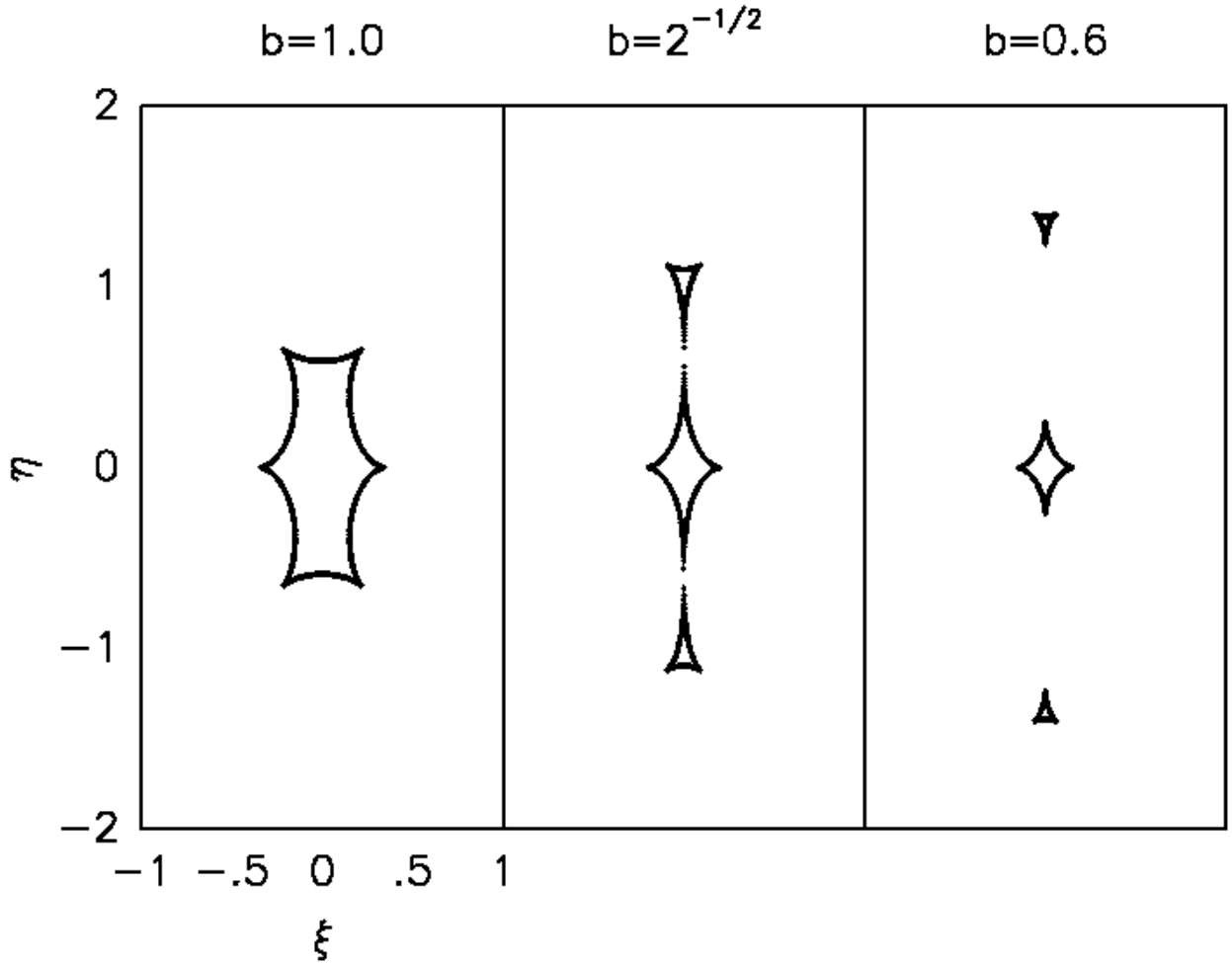
Figure 3. Caustic curves, defined as the locus of points in the source plane where the magnification is formally infinite, for binary separations of $b = 1.0, 2^{-1/2}, 0.6$.

and below the main caustic. As b decreases from $b = 0.7$, the secondary caustics become smaller and move farther from the center of mass, but the $\epsilon = 0.1$ contour still extends between the primary and secondary caustics. At $b \sim 0.5$, the $\epsilon = 0.1$ contour breaks, and no longer extends between the primary and secondary caustics. Thus the binary detection probability shown in Figure 2 exhibits a sharp break at
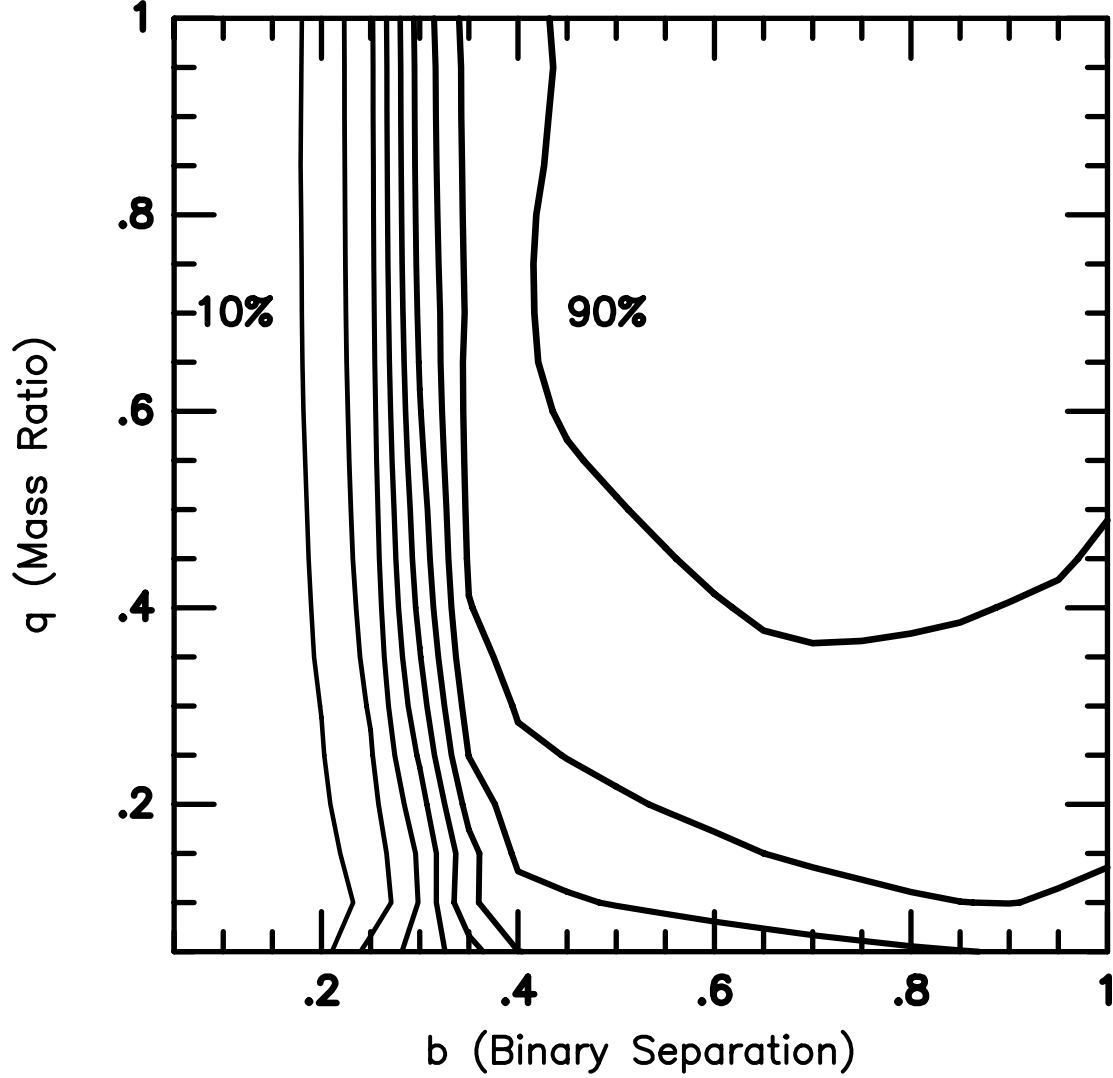
Figure 4. Contours of detection probability as a function of binary separation and mass ratio for $\epsilon_{thres} = 0.03$. Contours have equal spacings of 10%. A binary is considered detected if $|\epsilon| > 0.03$ at any point during the event.

$b \sim 0.5$, and declines rapidly for $b < 0.5$, as the primary caustic shrinks.

Figure 4 shows contours of binary detection probability as a function of b and q for $\epsilon_{thres} = 3\%$. Again, P is much more sensitive to b than q, and declines rapidly for $b < 0.4$. The reasons for the structure of Figure 4 are similar to those for

$\epsilon_{thres} = 3\%$, but note from Figure 1 that the $\epsilon = 0.03$ contours follow the structure of the caustics less closely, and thus the break in the detection probability occurs at a smaller value of b.

5. Orbital Motions

To understand the effect of the orbital motion of the binary on the detection probability, we define a parameter ψ, which describes the amount the binary rotates during the event,

$$\psi = 2\pi \frac{t_e}{P}, \tag{5.1}$$

where P is the period of the binary. Using Kepler's laws, and assuming face-on circular orbits and $D_{OS} \sim 8\,\mathrm{kpc}$, ψ can be written as,

$$\psi = \left(\frac{15\,\mathrm{km\,s}^{-1}}{v}\right)\left(\frac{M}{M_\odot}\right)^{1/4} [4z(1-z)]^{1/4} b^{-3/2}. \tag{5.2}$$

For $v \sim 200\,\mathrm{km\,s}^{-1}$, $z = 1/2$, and $M \sim 0.4 M_\odot$, this becomes $\psi \sim 0.06 b^{-3/2}$. Therefore, for $b > 0.3$, the binary will rotate by $\psi \lesssim 20°$. Thus the rotation of the binary during an event is small for most events, and will not change significantly the binary detection probabilities. This result is borne out quantitatively in numerical simulations that we have performed, but which we do not report in detail.

6. Finite Source Effects

In order to utilize microlensing as a method to reconstruct a mass function, one must be able to gather additional information for each individual event. One of the two necessary pieces of information is the proper motion of the lens, $\mu = v/D_{OL}$. For events with relatively small Einstein rings, (which are typically associated with the low-mass lenses considered here), μ can be measured primarily when the source passes very close to the lens. The light curve then deviates from that of a point source, and this deviation can then be used to determine μ.

12

It is therefore interesting to restrict consideration to those events for which finite source effects must be taken into account, and to ask what is the probability of detecting a binary if these effects are present. Since the majority of source stars for these events will be giants, we consider a source of average giant radius $R = 22R_\odot$ (Gould 1995b). For $D_{\rm OS} = 8\,{\rm kpc}$, $D_{\rm OL} = 4\,{\rm kpc}$, and $M \sim 0.4M_\odot$, this corresponds to a projected distance on the source plane, normalized to r_e, of $\rho = 0.03$. Gould & Welch (1996) estimate that, using optical/infrared photometry, proper motions could be measured when $\beta \lesssim 2\rho$. We therefore restrict our attention to those trajectories for which $\beta \le 0.06$. In general, when a source crosses a caustic, the magnification will deviate dramatically from that of a point mass lens, and the binary will be easily detectable. However, if the size of the caustic, which we will denote as w, is smaller than that of the source,

$$w \lesssim \rho, \tag{6.1}$$

then finite source effects will mask the binary magnification signature. If the caustics is very much smaller than the source, $w \ll \rho$, then the light curves for the binary and point-mass lenses will appear nearly identical when finite source effects are included. For $b \le 0.3$, the primary caustic is diamond-shaped, and it can be shown analytically that,

$$w \simeq b^2/2. \tag{6.2}$$

Combining equations (6.1) and (6.2), we find that finite source effects will partially mask the binary for $b \lesssim 0.25$.

To be more quantitative, we again calculate the excess magnification, ϵ, over a point lens [c.f. eq. (4.1)], where now A and A_0 are the magnifications of a finite source of radius $\rho = 0.03$. In order to calculate this magnification, we must integrate over the source. This could in principle be done directly in the source plane, but would prove difficult because the magnification diverges as the source position approaches the caustic. We therefore employ the method suggested by Bennett
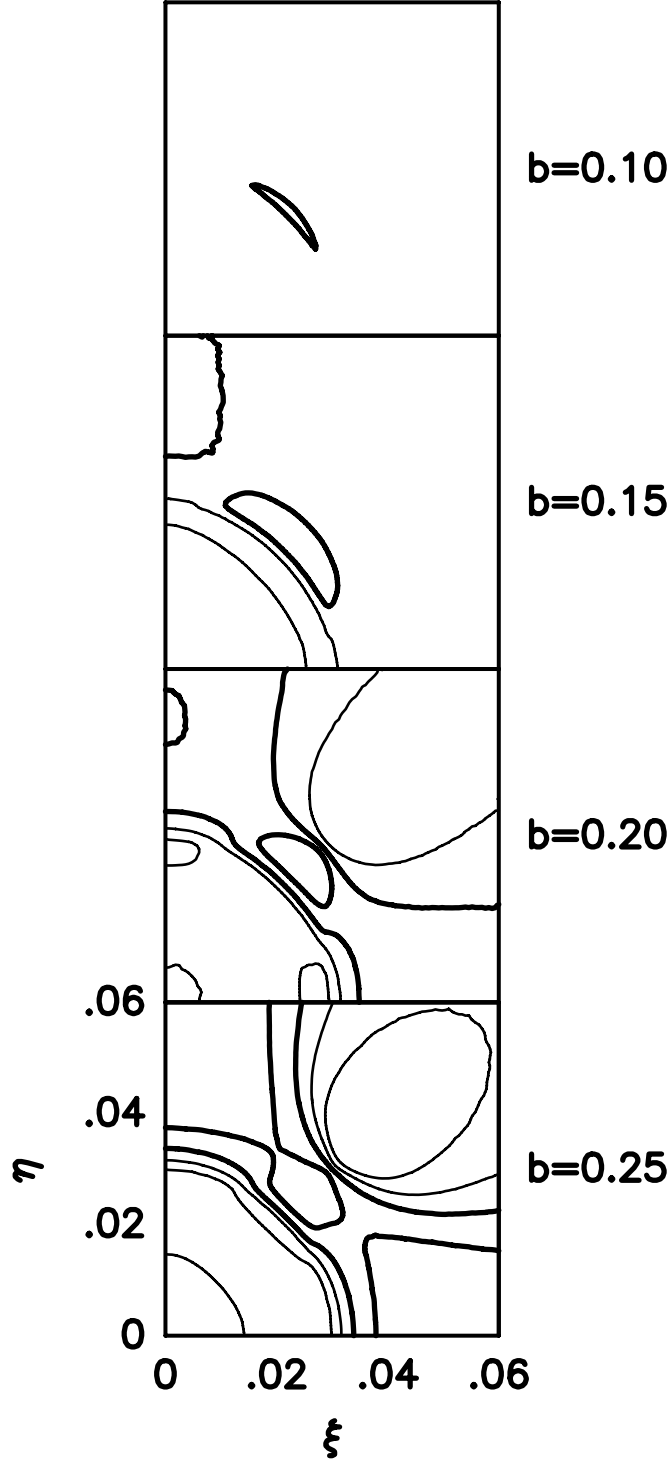
Figure 5. Contours of excess magnification, $\epsilon = \pm 0.03, \pm 0.10$, for a source of radius $\rho = 0.03$ for events with $|\zeta| \leq 0.06$ for binary separations of $b = 0.25, 0.20, 0.15, 0.10$. Positive contours are bold.
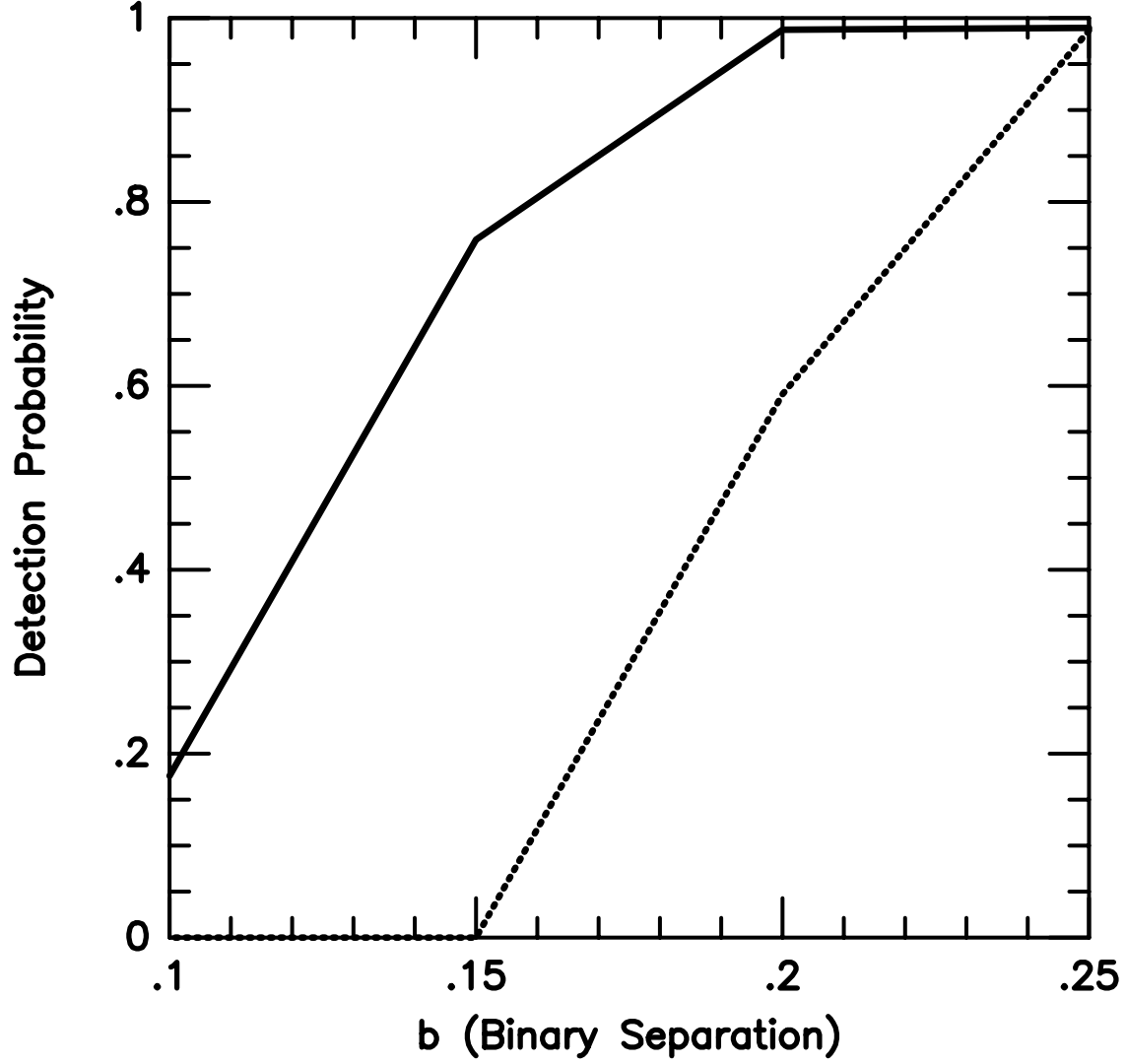
Figure 6.   Contours of detection probability as a function of binary separation for $\epsilon_{thres} = 0.03$(solid), 0.10(dashed). The source size is $\rho = 0.03$. A binary is considered detected if $|\epsilon| > \epsilon_{thres}$ at any point during the event.

& Rhie (1996), of integrating in the image plane, where the magnification is well behaved. In this case, the magnification is simply given by,

$$A = \frac{\sum_{i=1}^{n} \Omega_i}{\Omega_s},$$

(6.3)

where Ω_i is the area of image i, and $\Omega_s = \pi \rho^2$ is the area of the source. The diffi-

culty, therefore, lies in finding the images, which in general are scattered throughout the image plane. Fortunately, for $b \leq 0.3$, and $|\zeta| \leq 0.06$, the images are all confined to a thin annulus of radius $|\zeta| = 1$ for both the binary and single lens. Using this method, we now construct contours of ϵ as a function of position in the source plane, ζ, for a range of binary separations. In Figure 5 we show contours of $\epsilon = 0.03$ and 0.10 for $b = 0.10, 0.15, 0.20, 0.25$. Since the binary detection probability depends more strongly on b than q, we have included only the results for $q = 1.0$. The results for other mass ratios are qualitatively similar.

As in §3, we calculate the binary detection probability by integrating over lens trajectories in the intervals $0 \leq \theta \leq 2\pi$ and $0 \leq \beta \leq 1$. In Figure 6 we show the binary detection probability as a function of b for the range $0.10 \leq b \leq 0.25$. Figure 6 shows that finite source effects decrease the detection probability for $b < 0.25$, and render the binary virtually undetectable for $b \lesssim 0.1$, confirming the analytic estimate below equation (6.1).

7. Extreme Microlensing and Binary Detection

There exists a small subclass of events in which it is possible to measure both the proper motion, μ, and the projected Einstein radius, $\tilde{r}_e$, from ground-based measurement alone, and thus determine the mass of the lens. These extreme microlensing events (EMEs) have been discussed by Gould (1996b), and are characterized by a very high maximum magnification $A_{\max}$. The basic requirement to be able to measure μ and $\tilde{r}_e$ is, $A_{\max} \gtrsim 200$, and,

$$\beta \lesssim \rho. \tag{7.1}$$

We now determine whether it is possible to detect the presence of a binary of a given separation for these types of events. Gould (1996b) found that the typical source stars for EMEs are solar-type stars. For a source of physical radius $R \sim R_\odot$, the dimensionless radius is $\rho \simeq 0.001$ for $M = 0.4 M_\odot$, $D_{\mathrm{OL}} = 4\,\mathrm{kpc}$, and $D_{\mathrm{OS}} = 8\,\mathrm{kpc}$.

16

From equation (6.1), we estimate that the binary will still be detectable as long as $w \geq 0.001$. Using the relation (6.2), it is apparent that binaries of separation $b \gtrsim 0.05$ will be detectable in all EMEs. In fact, binaries of somewhat smaller separations will still be detectable, since as mentioned in §6, the requirement that $w \geq \rho$ is only approximate. Furthermore, to measure r_e, the sampling rate for EMEs must be very high, typically one observation per minute, with photometric precisions of $\leq 1\%$. With such observations, one would be able to detect binaries of much smaller separations, perhaps down to $b \sim .01$.

REFERENCES

1. Alard, C. 1996, in Proc. IAU Symp. 173 (Eds. C.S. Kochanek, J.N. Hewitt), in press (Kluwer Academic Publishers)

2. Alcock, C., et al. 1995, ApJ, 454, L125

3. Alcock, C., et al. 1996, ApJ, submitted (astro-ph=9606012)

4. Aubourg, E., et al. 1995, A&A, 301, 1

5. Bennett, D. & Rhie, S. 1996, preprint (astro-ph=9603158)

6. Boutreux, T. & Gould, A. 1996, ApJ, 462, 705

7. Buchalter, A. & Kamionkowski, M. 1996, ApJ, submitted (astro-ph=9604144)

8. Fischer, D. & Marcy, G. 1992, ApJ, 396, 178

9. Gaudi, B. S., & Gould, A. 1996, ApJ, submitted (astro-ph=9601030)

10. Gould, A. 1992, ApJ, 392, 442

11. Gould, A. 1994, ApJ, 421, L71

12. Gould, A. 1995a, ApJ, 441, L21

13. Gould, A. 1995b, ApJ, 447, 491

14. Gould, A. 1996a, PASP, 108, 465

15. Gould, A. 1996b, ApJ, submitted (astro-ph=9603148)

16. Gould, A. & Welch, D. 1996, ApJ, 464, 212

17. Kroupa, P., Tout, C., & Gilmore, G. 1991, 251, 293

18. Marcy, G. & Benitz, K. 1989, ApJ, 344, 441

19. Nemiroff, R. J. & Wickramasinghe, W. A. D. T. 1994, ApJ, 424, L21

20. Refsdal, S. 1966, MNRAS, 134, 315

21. Reid, N. 1991, AJ, 102, 1428

22. Udalski, A., et al. 1994, ApJ, 436, L103

23. Witt, H., & Mao, S. 1994, ApJ, 430, 505

24. Witt, H. 1990, A&A, 236, 311